The correlation between the optical absorption spectrum and paramagnetic properties of neodymium trifluoride

1994 J. Phys.: Condens. Matter 6 5169

(http://iopscience.iop.org/0953-8984/6/27/025)

J. Phys.: Condens. Matter 6 (1994) 5169–5180. Printed in the UK

The correlation between the optical absorption spectrum and paramagnetic properties of neodymium trifluoride

L Beaury, J Derouet, M Escorne and P Porcher
Laboratoire de Chimie Métallurgique et Spectroscopie des Terres Rares, UPR, 209 du CNRS, 1 Place A Briand, 92195 Meudon, France

Received 7 February 1994, in final form 21 March 1994

Abstract. The $4f^3$ configuration of Nd^{3+} in NdF_3 has been revisited. The real point symmetry of the crystalline matrix—C_2—has been considered for the simulation, which means 15 crystal field parameters (CFPs). The simulation has been conducted by considering together the energy level scheme derived from the optical absorption spectra *and* the paramagnetic susceptibility and its variation with the temperature *and* the g values of the ground level. It is shown that only a single set of CFPs reproduces this information correctly, whereas various sets are found if only the energy level scheme is retained in the simulation process.

1. Introduction

The rare earth trifluoride is one of the most completely studied crystalline matrices, in terms of determination of the energy level scheme of the $4f^N$ configurations. This exceptional feature is due to (i) the facility to grow single crystals, (ii) very good transparency far into the UV region, which provides a great number of experimental levels, and (iii) the fact that the rare earth trifluorides constitute an isostructural series for most of the rare earths. Consequently, this matrix provides one of the best opportunities for testing the simulation models derived from theories of atomic spectra. Among these fluorides the energy level sequence of Nd^{3+} ($4f^3$) is certainly the most interesting as a consequence of a relatively large number of configuration states (182 Kramers doublets), but not too large in terms of the size of the secular determinant we need to diagonalize. The energy level scheme of LaF_3:Nd^{3+} has been previously reported by Carnall *et al* [1] (146 crystal field levels were experimentally obtained and fitted to a root mean square deviation of 14.0 cm^{-1}) and also by some of us [2] (116 levels among the 127 observed levels were fitted to a mean square deviation of 15.5 cm^{-1}). These two simulations were performed by considering a crystal field Hamiltonian with a C_{2v} symmetry, an approximation of C_2, the real point symmetry of the site occupied by the Nd [3].

The aim of the present work is to revisit the energy level scheme deduced from the optical absorption spectrum and to reproduce the position of the 137 observed energy levels by considering the real site symmetry C_2 (table 1). As a second step, the derived wavefunctions have been used for calculating the paramagnetic susceptibility and its evolution versus temperature and the g values of the ground state level. The comparison with experimental measurements performed on a single crystal constitutes an excellent opportunity to test the ability of the model to give 'good' wavefunctions for the ion considered. The most sensible test is the reproduction of the g value characteristic of the ground crystal field level, whereas the calculated paramagnetic susceptibility includes contributions from different levels, which has the disadvantage of averaging the values.

0953-8984/94/275169+12$19.50

Table 1. Experimental and calculated energy levels and computed g values for Nd^{3+} in NdF_3 (from set No 1).

Nominal state $^{2S+1}L(v)_J$	E_{exp} (cm^{-1})	E_{calc} (cm^{-1})	$\lvert g_{\parallel}\rvert$ (calc)	$\lvert g_{\perp 1}\rvert$ (calc)	$\lvert g_{\perp 2}\rvert$ (calc)
$^4I_{9/2}$	0	−13	3.02	1.72	1.03
	38	17	2.14	2.82	0.01
	142	139	1.18	1.85	0.14
	331	317	0.56	3.98	3.06
	522	515	4.01	2.10	1.63
$^4I_{11/2}$	—	1971	10.05	0.44	0.14
	—	2021	1.82	2.57	5.53
	—	2058	1.52	2.70	6.46
	—	2112	0.96	9.43	1.07
	—	2203	2.71	1.67	5.67
	—	2232	7.55	3.39	1.72
$^4I_{13/2}$	3929	3918	13.59	0.72	0.06
	3982	3973	1.16	3.89	8.64
	4052	4033	0.66	1.81	7.57
	4090	4108	0.84	11.47	2.44
	4131	4142	2.69	4.52	7.86
	4210	4224	5.84	0.63	3.65
	4305	4300	10.43	3.14	2.41
$^4I_{15/2}$	5808	5816	7.19	3.42	6.63
	5882	5881	7.95	4.67	1.45
	5996	6001	2.97	2.35	3.42
	6181	6188	1.65	8.78	6.24
	—	6229	0.49	7.57	8.37
	6344	6341	2.35	2.21	5.86
	6500	6510	6.01	7.25	2.50
	6590	6610	12.25	5.05	3.14
$^4F_{3/2}$	11 600	11 569	0.38	1.04	0.16
	11 646	11 627	0.71	0.51	0.90
$^4F_{5/2}$ & $^2H(2)_{9/2}$	12 600	12 583	2.47	2.52	0.63
	12 614	12 606	2.46	3.47	0.79
	12 658	12 646	0.45	3.25	3.99
	12 684	12 675	2.26	1.15	0.16
	12 703	12 707	0.67	3.25	3.95
	12 770	12 802	2.36	2.23	0.59
	12 860	12 901	2.54	0.46	1.95
	12 923	12 919	3.35	2.20	3.19
$^4F_{7/2}$ & $^4S_{3/2}$	13 521	13 518	2.49	2.93	0.45
	13 604	13 616	1.48	2.21	3.39
	13 671	13 695	0.71	2.12	4.93
	13 691	13 717	1.92	5.20	1.14
	13 738	13 723	4.49	2.16	2.96
	13 738	13 758	0.51	1.51	3.96
$^4F_{9/2}$	14 846	14 861	0.86	10.10	0.82
	14 870	14 882	10.74	1.12	0.11
	14 912	14 915	2.01	6.45	1.33
	14 941	14 953	4.19	4.00	1.14
	14 972	14 984	7.40	2.54	2.78

Table 1. (continued)

Nominal state $^{2S+1}L(v)_J$	E_{exp} (cm^{-1})	E_{calc} (cm^{-1})	$\lvert g_{\parallel}\rvert$ (calc)	$\lvert g_{\perp 1}\rvert$ (calc)	$\lvert g_{\perp 2}\rvert$ (calc)
$^2H(2)_{11/2}$	16003	16022	1.25	7.31	3.02
	16041	16037	6.93	3.23	0.78
	16057	16047	0.93	3.57	2.88
	16067	16067	1.96	3.44	0.01
	16111	16096	2.41	3.39	4.16
	16179	16144	7.68	2.35	1.75
$^4G_{5/2}$ &	17313	17307	0.71	0.57	0.19
$^4G_{7/2}$ &	17319	17331	0.49	1.21	0.22
$^2G(1)_{7/2}$	17376	17377	1.06	0.28	0.74
	17525	17509	2.47	1.98	2.93
	17535	17521	2.37	1.17	0.54
	17590	17582	1.94	1.38	1.49
	17621	17617	1.73	0.85	1.60
	19150	19126	3.68	1.49	1.57
	19238	19218	0.84	5.12	0.15
	19260	19272	0.56	2.25	2.77
	19342	19338	3.85	1.20	0.41
$^2K_{13/2}$ &	19585	19609	10.65	1.56	0.96
$^4G_{9/2}$	19612	19635	1.85	1.13	8.35
	19658	19679	3.92	2.77	2.16
	19689	19712	4.93	2.05	1.81
	19712	19740	5.32	2.82	2.66
	19751	19768	5.08	3.96	1.46
	—	19786	1.00	0.71	0.55
	19806	19807	1.37	0.88	0.63
	19849	19868	1.21	5.17	2.25
	19897	19920	5.39	2.44	0.62
	19980	19969	4.24	8.43	1.31
	—	20046	5.79	8.81	0.67
$^2G(1)_{9/2}$	21160	21140	3.60	6.56	1.46
	21177	21174	2.29	5.38	2.94
	21200	21194	1.55	5.97	1.57
	21236	21221	2.20	0.17	3.32
	21259	21268	2.56	0.67	2.19
$^2D(1)_{3/2}$	21340	21331	0.70	0.45	0.22
	21354	21345	0.60	0.92	0.55
$^4G_{11/2}$ &	—	21623	2.84	4.19	4.11
$^2K_{15/2}$	21687	21667	6.34	0.74	1.18
	21725	21705	2.65	3.56	6.96
	21777	21754	2.95	4.29	0.42
	21786	21784	2.06	5.46	0.43
	21815	21829	6.86	1.45	0.87
	21853	21853	4.63	3.14	3.53
	—	21887	6.73	2.72	2.24
	21901	21897	2.99	2.83	0.80
	21944	21927	2.29	6.91	1.30
	21964	21958	8.45	1.07	2.36
	21993	21981	3.91	4.10	2.04
	22007	22028	4.28	8.57	3.94
	—	22089	3.40	9.69	3.39

Table 1. (continued)

Nominal state $^{2S+1}L(v)_J$	E_{exp} (cm^{-1})	E_{calc} (cm^{-1})	$\lvert g_{\parallel}\rvert$ (calc)	$\lvert g_{\perp 1}\rvert$ (calc)	$\lvert g_{\perp 2}\rvert$ (calc)
$^2P_{1/2}$	23471	23472	0.62	0.64	0.62
$^2D(1)_{5/2}$	23952	23940	1.82	5.65	0.41
	24004	24020	0.30	3.64	0.65
	24056	24061	3.73	1.42	3.36
$^2P_{3/2}$	26350	26340	0.80	3.18	0.25
	26406	26398	1.90	1.16	2.44
$^4D_{3.2}$	28313	28329	2.92	2.30	0.28
	28361	28372	2.11	2.42	0.52
$^4D_{5/2}$	28498	28488	4.27	0.26	1.53
	28522	28525	2.01	1.95	2.18
	28653	28654	4.11	1.33	1.46
$^4D_{1/2}$	28952	28987	0.20	0.39	0.21
$^2I_{11/2}$	29429	29419	6.97	4.33	2.10
	29455	29460	6.03	1.83	0.16
	29533	29527	3.76	4.32	1.58
	29603	29617	6.44	1.42	1.10
	—	29631	1.86	4.66	0.46
	29753	29764	0.79	9.04	1.49
$^2L_{15/2}$ & $^4D_{7/2}$	30221	30198	7.96	1.67	5.38
	30248	30252	1.14	1.57	4.04
	30312	30321	10.82	0.18	2.66
	30403	30409	3.79	9.17	0.21
	30432	30456	4.51	6.19	2.95
	30525	30498	4.41	6.99	0.82
	30544	30528	5.30	2.46	4.13
	30572	30576	2.61	6.54	0.74
	30637	30594	3.83	4.14	1.01
	30665	30662	4.98	4.66	2.24
	30769	30762	3.01	12.21	0.34
	—	30776	1.25	9.25	0.37
$^2I_{13/2}$	30845	30854	9.35	5.20	2.82
	30941	30904	4.08	3.56	5.26
	30998	30963	1.04	7.42	0.10
	31024	31028	10.11	0.14	1.74
	—	31050	2.16	7.35	2.95
	—	31085	0.89	8.51	0.57
	31133	31151	1.23	12.96	0.34
$^2L_{17/2}$	31736	31743	13.11	2.35	2.90
	—	31775	1.17	1.24	12.66
	31847	31828	15.85	0.64	1.06
	—	31943	4.70	2.30	8.76
	—	31952	3.96	11.42	2.09
	—	31966	2.80	9.98	2.02
	—	32038	5.35	10.81	2.33
	—	32113	4.33	13.40	0.73
	—	32250	4.25	16.40	0.04
$^2H(1)_{9/2}$	32992	32984	4.69	1.72	3.18
	33058	33068	1.32	2.38	3.62
	33146	33155	5.14	2.12	1.13
	33200	33197	2.87	0.84	3.78
	33234	33231	0.83	4.20	0.23

Table 1. (continued)

Nominal state $^{2S+1}L(v)_J$	E_{exp} (cm^{-1})	E_{calc} (cm^{-1})	$\lvert g_{\parallel}\rvert$ (calc)	$\lvert g_{\perp 1}\rvert$ (calc)	$\lvert g_{\perp 2}\rvert$ (calc)
$^2D(2)_{3/2}$	33 568	33 571	1.02	0.99	1.96
	33 602	33 607	0.85	2.48	0.38
$^2H(1)_{11/2}$ &	34 235	34 225	5.54	1.96	2.60
$^2D(2)_{5/2}$	34 341	34 337	0.61	1.76	1.39
	34 376	34 394	5.29	0.39	0.28
	34 471	34 482	3.80	3.47	2.48
	—	34 506	2.30	1.92	3.31
	34 590	34 555	1.15	2.53	1.45
	34 650	34 677	3.65	3.53	1.01
	34 686	34 700	6.66	0.13	0.57
	—	34 822	2.92	4.41	3.47
$^2F(2)_{5/2}$	38 640	38 656	3.34	0.91	1.88
	38 700	38 708	0.64	2.36	1.65
	38 820	38 789	1.80	3.79	0.63
$^2F(2)_{7/2}$	—	40 060	2.95	1.42	0.49
	—	40 100	1.29	2.60	1.31
	—	40 160	0.96	5.69	2.10
	—	40 224	4.27	1.96	1.79
$^2G(2)_{9/2}$	—	47 860	4.35	1.15	4.25
	—	47 880	3.62	1.64	4.39
	—	47 953	3.18	0.18	1.93
	—	48 039	4.86	4.60	1.82
	—	48 087	1.47	8.42	1.55
$^2G(2)_{7/2}$	—	48 727	1.62	1.29	1.61
	—	48 770	0.27	2.72	1.09
	—	48 905	1.49	2.45	0.92
	—	48 994	1.35	4.71	2.01
$^2F(1)_{7/2}$	—	66 359	4.14	1.40	3.41
	—	66.519	3.01	2.29	0.32
	—	66 614	3.68	2.93	2.32
	—	66 787	1.18	7.52	0.67
$^2F(1)_{5/2}$	—	67 673	1.92	1.08	2.88
	—	67 793	2.54	1.57	0.96
	—	68 034	0.80	3.89	0.82

2. Optical spectrum and simulation

We have revisited the optical absorption spectrum of pure NdF_3 as a single crystal up to 38 900 cm^{-1} at liquid He temperature. The experimental conditions have been described elsewhere [2]. 138 levels are observed (table 1); only one of them is not very certain and is thus not included in the simulation. In this matrix some of the energy levels located in the UV energy range are observed ($^2H(1)_{9/2}$, $^2D(2)_{3/2}$, $^2H(1)_{11/2}$, $^2D(2)_{5/2}$ and $^2F(2)_{5/2}$, which allows us to vary freely all the free ion parameters.

2.1. *Theoretical treatment of experimental optical data*

The central field approximation considers separately the Hamiltonians corresponding to the free ion and crystal-field interactions, although the final purpose is to input them simultaneously in the secular determinant before diagonalization. The major free ion interactions in the trivalent rare earth ions with the $4f^N$ configurations include the electrostatic repulsion between the 4f electrons and the coupling of their spin and orbital angular momenta. Several minor contributions within the free ion scheme can be taken into account in addition to the crystal field effect. Since the treatment of these primary and other smaller but essential contributions to the effective operator Hamiltonian of the system has been covered in an extensive review [4], we limit our discussion to an identification of the parameters and the corresponding operators of the parametric model. The Hamiltonian used in the present study can be written as

$$H = H_0 + \sum_{k=0,1,2,3} E_k(nf, nf)e^k + \zeta_{4f}A_{SO} + \alpha L(L+1) + \beta G(G_2) + \gamma G(R_7) + \sum_{\lambda=2,3,4,6,7,8} T^\lambda t_\lambda + H_{CF}.$$

H_0 is the spherically symmetric one-electron part of the free ion Hamiltonian, which separates the ground configuration from excited ones, E_k are the Racah parameters, ζ_{4f} is the spin–orbit coupling constant and e^k and A_{SO} represent the angular parts of the electrostatic repulsion and spin–orbit coupling respectively. For the configurations of two or more equivalent electrons the two-body interactions must be taken into consideration; they introduce the Tree parameters α, β and γ; L is the total orbital angular momentum; $G(G_2)$ and $G(R_7)$ are the Casimir operators for the groups G_2 and R_7 respectively. For configurations with three or more equivalent 4f electrons, we can apply the three-body configuration interaction terms parametrized with the Judd's parameters $T^\lambda (\lambda = 2, 3, 4, 6, 7, 8)$; the t_λ are operators transforming according to the irreducible groups G_2 and R_7, also. In our simulation the magnetic interactions (spin–spin, spin–other orbit) parametrized by the M^k and P^k integrals are not included [1].

The one-electron crystal field Hamiltonian H_{CF} [5] consists of a sum of products between the real and imaginary parts of the crystal field parameters (CFPs) B^k_q and S^k_q and the spherical harmonics C^k_q as follows:

$$H_{CF} = \sum_{k=0}^{6} \sum_{q=-k}^{k} [B^k_q(C^k_q + (-1)^q C^k_{-q}) + iS^k_q(C^k_q - (-1)^q C^k_{-q})].$$

The number of non-zero real and imaginary parameters depends on the crystallographic point site symmetry of the lanthanide ion. For a C_{2v} point symmetry nine non-zero B^k_q CFPs are involved whereas nine non-zero B^k_q CFPs and six non-zero S^k_q CFPs are necessary to describe the C_2 point symmetry. Usually when crystal field calculations are performed with a C_2 point symmetry S^2_2 is set to zero, which corresponds to an arbitrary choice of the (x, y) reference axis system. This is no longer possible here because the magnetic data suppose a precise orientation of the axis set; thus S^2_2 is included in some simulations. The two-electron crystal field parameters are set to zero and do not vary in this simulation.

2.2. *Simulation*

The actual fitting procedure between experimental and calculated energy level values was conducted with standard least-squares calculations using the root mean square (RMS) standard deviation as a figure of merit describing the quality of the fit:

$$\sigma = (\Sigma(E_{exp} - E_{calc})^2/(N_{lev} - N_{par}))^{1/2}$$

where E_{exp} and E_{calc} are the experimental and calculated energies, N_{lev} is the number of experimental levels and N_{par} the number of parameters. Although the calculation was executed in the approximate symmetry C_{2v}, Carnall *et al* [1] found a good agreement between experimental and calculated energy levels; however, this set of parameters will appear as not satisfactory in the sense that it is not able to reproduced *at the same time* the energy level scheme *and* g values *and* the paramagnetic susceptibility and its evolution versus temperature. One fitting was attempted in symmetry C_2 by Morrison and Leavitt [6] but only with 47 levels. Another simulation performed more recently by Duan and Xu [7], also considering a strongly reduced basis, yielded completely different values for the CFPs, apparently non-realistic. In our fitting procedure on the real point symmetry C_2, the initial CFP values are those of [2] for the free ion parameters as well as for the B_q^k CFPs. The starting S_q^k values are those deduced from the lattice sum calculation of Morrison and Leavitt reported by Carnall [1], which was based on the crystal structure of Cheetham *et al* [3].

A simulation involving so many parameters is rather difficult to perform in terms of significance of the parameters and of their certainty. The problem becomes serious when the symmetry is relatively low, because the CFPs have individually a smaller influence on the energy levels positions than the free ion parameters. Several sets of CFPs can be found. It is obvious that the final result will always depend on the choice made for the refinement. An alternative method for the simulation is to consider the descending symmetry procedure, by which the final and real symmetry is considered as distorted from higher symmetry. In the case of NdF$_3$, the procedure could be $D_{3h} \rightarrow D_3 \rightarrow C_{2v} \rightarrow C_2$. The simulation in the D_{3h} point symmetry involves only four real CFPs, which gives a relatively simple and certain simulation procedure. After that, the CFPs are transformed according to a rotation, making the reference z axis of the crystal field potential collinear with the C_2 axis of the structure, which gives two sets of starting parameters for the C_{2v} point symmetry [8] and finally the imaginary parts of the CFPs are added in the last step of the simulation, in the C_2 symmetry.

The first step of the simulation is to operate in the C_{2v} symmetry. The set A obtained in [2] from 116 energy levels was used as starting values for the simulation running on 137 energy levels; the set B was then deduced.

In the second step, the simulation operates in C_2 symmetry, using the set B as initial values. For a refinement involving many CFPs the parameters are never *all* varied simultaneously. Some of them are allowed to vary, others being fixed in a more or less arbitrary manner. The real parts of the CFPs are first fixed and the imaginary parts are varied; after that, only the real parts are varied, the imaginary parts being fixed, and the iteration is carried on up to the final set of parameters. In fact, we found four sets of CFPs in C_2 symmetry not fundamentally different from each other (with the exception of the set No 4, from the second way in the $D_{3h} \rightarrow D_3 \rightarrow C_{2v}$ path [8], giving almost the same RMS standard deviations (between 17.7 and 18.4 cm^{-1}), but without any significant variation in the energy level scheme. They can be considered as solutions for the simulation from the optical data (table 2).

3. Paramagnetic susceptibility and its simulation

For the following discussion we have to keep in mind that the real site symmetry of NdF$_3$ is C_2 [3], but distortion of a D_3 site. Our reference axis is the pseudo-threefold axis and we call the susceptibility obtained when the magnetic field is parallel to this threefold axis $\chi_{\parallel}$.

Table 2. Free ion and crystal field parameters for Nd^{3+} in NdF_3. Values are in cm^{-1}. Sets 1 to 4 represent different steps in the refinement procedure (see the text).

Parameter	Set A (C_{2v}) from [2]	Set B (C_{2v})	Set No 1	Set No 2	Set No 3	Set No 4
E^0	23 869(2)	23 826(1)	23 826(2)	23 827(1)	23 820(1)	23 830(1)
E^1	4839(3)	4823(1)	4822(1)	4824(1)	4821(1)	4823(1)
E^2	23.79(0.04)	23.70(0.01)	23.70(0.01)	23.70(0.01)	23.70(0.01)	23.72(0.01)
E^3	*490(1)*	*490.4(0.1)*	*490.2(0.2)*	*490.5(0.1)*	*489.6(0.1)*	*490.5(0.2)*
ζ	880(1)	881.7(1.0)	881.6(0.7)	881.6(0.7)	881.2(0.7)	881.0(0.7)
α	20.8(0.2)	21.28(0.03)	21.27(0.03)	21.28(0.03)	21.39(0.03)	21.10(0.03)
β	−581(11)	−576(4)	−575(3)	−576(3)	−580(3)	−571(3)
γ	[1443]	1514(3)	1515(4)	1509(4)	1518(4)	1512(4)
T^2	312(34)	304(3)	309(3)	302(3)	327(2)	296(3)
T^3	47(4)	43(2)	43(2)	43(2)	42(2)	43(2)
T^4	94(4)	95(2)	96(2)	95(2)	98(2)	101(2)
T^6	−276(9)	−301(5)	−300(4)	−301(5)	−302(5)	−301(5)
T^7	304(17)	323(5)	326(5)	325(5)	335(5)	325(5)
T^8	264(27)	237(6)	236(6)	232(6)	255(6)	227(6)
B^2_0	117(25)	193(14)	184(15)	185(15)	191(14)	122(14)
B^2_2	−215(23)	−220(7)	−208(7)	−225(7)	−262(6)	201(7)
B^4_0	361(46)	241(44)	276(48)	217(47)	251(49)	299(58)
B^4_2	421(65)	544(26)	482(28)	502(28)	518(28)	−390(30)
B^4_4	586(54)	550(24)	599(24)	489(28)	429(28)	684(23)
B^6_0	−1224(50)	−1208(33)	−1203(33)	−1222(33)	−1073(37)	93(45)
B^6_2	149(72)	173(30)	168(35)	234(31)	91(33)	1177(18)
B^6_4	−1035(42)	−953(20)	−892(30)	−856(23)	−568(31)	−151(40)
B^6_6	−546(38)	−594(28)	−602(30)	−382(40)	−664(29)	689(26)
S^2_2	—	—	113(14)	[0]	21(14)	[0]
S^4_2	—	—	−16(45)	142(53)	60(47)	−73(64)
S^4_4	—	—	−73(47)	302(41)	321(35)	175(53)
S^6_2	—	—	346(40)	−232(42)	307(44)	361(46)
S^6_4	—	—	54(78)	−187(61)	−670(29)	186(40)
S^6_6	—	—	271(51)	−524(33)	−414(41)	−163(65)
nb levels	116	137	137	137	137	137
RMS	15.5	18.4	18.3	18.1	17.7	18.4
Residue	22 736	38 706	36 142	35 952	33 983	37 075

Although the twofold axis—perpendicular to this pseudo-threefold axis—is the reference axis for the description of the crystal field potential and consequently for our calculations, all results will be presented versus the pseudo-threefold axis.

3.1. Experimental background

The paramagnetic susceptibilities have been measured on two sets of apparatus: the $\chi_\parallel$ and $\chi_\perp$ values were measured from 4.2 to 1100 K using a Faraday balance (figure 1); $\chi_{\perp 1}$ and $\chi_{\perp 2}$ are values measured in two mutually perpendicular directions, perpendicular to the applied magnetic field, measured on a DSM8 susceptometer from 2 to 300 K (figure 2). The set-up was calibrated with $BaFe_{12}O_{19}$ as standard. The diamagnetic correction was calculated using the values—in 10^{-6} emu mol^{-1}—of −27 and 9 for Nd^{3+} and F^-, respectively [9]. The magnetic susceptibilities were found to be independent of the magnetic field (up to 18 kG) in the temperature range measurement.

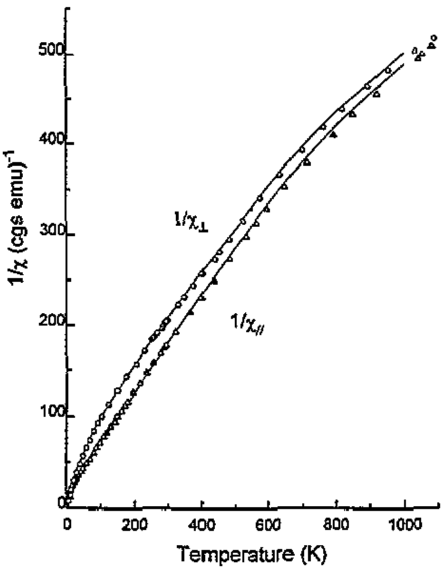

Figure 1. The paramagnetic susceptibility of NdF_3, parallel (triangles) and perpendicular (circles) to the C_3 axis, measured from 4.2 to 1100 K. Computed values (continuous line) are from set No 1.

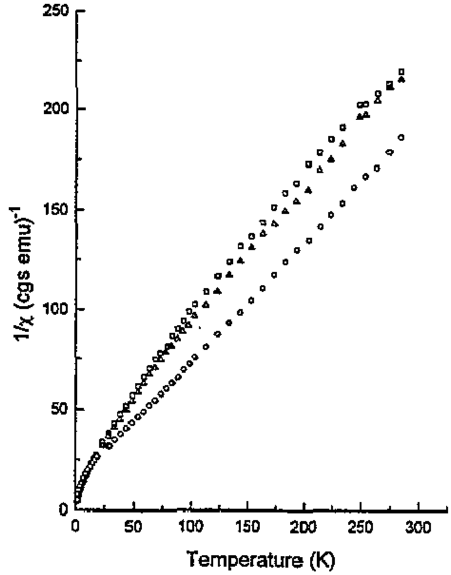

Figure 2. Experimental values ($\chi_\parallel$ (circles), $\chi_{\perp 1}$ (squares) and $\chi_{\perp 2}$ (triangles)) measured with the DSM8 susceptometer.

Picard *et al* [10] have determined with accuracy the values of $\chi_\parallel$ at very low temperature between 2 and 4.2 K. We have already reported these values in [2] (with an error for the $1/\chi_\parallel$ scale).

3.2. Computed values

An applied external magnetic field constitutes a new interaction operating as a perturbation of the system. Naturally, it is always possible to introduce the magnetic operator characterizing this perturbation in the secular determinant before diagonalization. The main effect should be to lift the remaining degeneracy of the Kramers doublets. This also means that we would need to diagonalize a matrix whose size has the configuration degeneracy, without any possible division into submatrices to save the computing time as well as to obtain more certainty in the wavefunctions. In fact, due to the relatively small amplitude of the usual magnetic field, the best way is to consider the Van Vleck formula [11], the result of an application of perturbation theory. The magnetic susceptibility χ is then written as

$$\chi = \left[N\beta^2 \Big/ \sum_i \exp - \left(\frac{E_i^{(0)}}{kT}\right)\right] \sum_i \left[\frac{(\varepsilon_i^{(1)})^2}{kT} - 2\varepsilon_i^{(2)}\right] \exp - \left(\frac{E_i^{(0)}}{kT}\right)$$

with

$$\varepsilon_i^{(1)} = \langle \Psi_i | (\boldsymbol{L} + g_e \boldsymbol{S}) \cdot \boldsymbol{u} | \Psi_i \rangle$$

and

$$\varepsilon_i^{(2)} = \sum_{\substack{j \\ E_i^{(0)} \neq E_j^{(0)}}} \frac{[\langle \Psi_i | (\boldsymbol{L} + g_e \boldsymbol{S}) \cdot \boldsymbol{u} | \Psi_j \rangle]^2}{E_i^{(0)} - E_j^{(0)}}.$$

Table 3. g values. Sets 1–4 represent different steps in the refinement procedure (see the text).

g	Experiment [15]	Experiment [13]	Set A (C_{2v}) from [2]	Set B (C_{2v})	Parameters from [1]	Set No 1	Set No 2	Set No 3	Set No 4
$\|g_{\parallel}\|$	3.02	3.11	2.73	2.89	3.53	3.02	2.13	3.50	0.26
$\|g_{\perp 1}\|$	1.72	1.36	2.37	1.11	1.78	1.72	2.47	1.58	3.32
$\|g_{\perp 2}\|$	1.03	1.09	1.99	0.16	1.39	1.03	1.26	1.01	0.29

In these expressions, N is the Avogadro number, k is the Boltzmann constant, β is the Bohr magneton and $g_e = 2.0023$. The wavefunctions Ψ_i and Ψ_j are the unperturbed eigenfunctions of the Hamiltonian, corresponding to the $E_i^{(0)}$ and $E_j^{(0)}$ eigenvalues. $\boldsymbol{u}$ is a unit vector related to the three susceptibilities χ_x, χ_y and χ_z.

The calculations have been performed by considering the 18 lowest Kramers doublets ($^4I_{9/2}, ^4I_{11/2}, ^4I_{13/2}$) which appeared to be largely sufficient to cover the thermal population effect well above 1000 K [12]. The results of this calculation is reported in figure 1; if the threefold axis is the z axis, $\chi_{\parallel} = \chi_z$ and $\chi_{\perp}$ is taken as $(\chi_x + \chi_y)/2$. There is a small deviation at $T > 800$ K, which may be due to a modification of the NdF_3 cell parameters and consequently of the CFPs. The reproduction of the experimental data is very good for three sets among four, with the exception of set No 4. At low temperatures set No 2 gives the best simulation. In contrast set No 3 is not satisfactory in that area, whereas set No 1 reproduces correctly the experimental data in the whole temperature range (figure 1). Finally we cannot determine which CFPs set is the best for this simulation.

4. g values and their simulation

4.1. Experimental data

The g values for the ground state level of Nd^{3+} in LaF_3 have been experimentally determined by electron spin resonance [13]: $g_{\parallel} = 3.11$, $g_{\perp 1} = 1.36$, $g_{\perp 2} = 1.09$. The value of $g_{\parallel}$ has been used for estimation of the spin–lattice relaxation time of Nd^{3+} in NdF_3 single crystals [14]. Moreover, the magnetic field dependence in a far-infrared spectrum study gave another set of values [15] close to the preceding one: $g_{\parallel} = 3.02$, $g_{\perp 1} = 1.72$, $g_{\perp 2} = 1.03$.

4.2. Computed values

The principle of g calculation is quite similar to that of paramagnetic susceptibility. The same $(\boldsymbol{L} + g_e\boldsymbol{S})$ tensorial operator is applied to the wavefunction of a level. The g values are non-zero only for Kramers doublets. When the symmetry is binary, as for NdF_3, the three components of g have relatively simple expressions:

$$g_{\parallel} = g_z = 2\langle\Psi_+|L_z + g_e S_z|\Psi_+\rangle$$

$$g_{\perp 1} = g_x = 2\langle\Psi_+|L_x + g_e S_x|\Psi_-\rangle$$

$$g_{\perp 2} = g_y = 2\mathrm{i}\langle\Psi_+|L_y + g_e S_y|\Psi_-\rangle.$$

In these expressions, Ψ_+ is one eigenvector of the form

$$\Psi_+ = a|J, M\rangle + b|J, M'\rangle + \cdots$$

and Ψ_- is its Kramers conjugate

$$\Psi_- = (-1)^{J+M} a^*|J, -M\rangle + (-1)^{J+M'} b^*|J, -M'\rangle + \cdots.$$

Table 3 reports the values of $|g_{\parallel}|$, $|g_{\perp 1}|$ and $|g_{\perp 2}|$ for the ground crystal field level calculated with the different sets of CFPs.

5. Discussion

Among the four sets of CFPs which give about the same RMS standard deviation for the fitting of the optical energy levels, only one of them (No 4) gives g and $\chi_\parallel$ values far from the experimental values and with even the anisotropy $1/\chi_\parallel - 1/\chi_\perp$ reversed when compared to the experiment. The other sets give a good general agreement for the paramagnetic susceptibility simulation. Set No 1 gives the best agreement for the whole temperature range whereas set No 2 reproduces $1/\chi_\parallel$ more precisely at very low temperature (2 K$< T <$ 4.2 K). This is due to (i) the almost perfect simulation of the energy difference between the ground and the first excited crystal field levels (36 cm^{-1} compared to the experimental value 38 cm^{-1}) and (ii) differences in the wavefunction composition. These two sets have exactly the same free ion parameters. For the g values the best agreement is obtained with set No 1, which is assumed to constitute the final result.

As mentioned before, these different sets of parameters confirm the difficulties for running a correct and certain simulation only by considering the optical data, when the number of parameters which have to vary freely is so large. In this sense the use of the g values as well as the χ values seems to be essential in order to achieve the simulation. It is also evident that such difficulties occur when the number of CFPs is large. For crystals with higher point symmetries, thus with fewer CFPs, the optical data can be sufficient for running a certain simulation. The same type of problem may also be found for the simulation of the $3d^N$ configurations [16, 17], which have generally an experimental energy level scheme reduced to a few bands. This is also the case of non-transparent rare earth materials, for which only some of the ground levels can be measured by neutron scattering [18]. One possible way to reproduce the behaviour of the $3d^N$ or $4f^N$ configurations in such cases is to include in the fitting procedure the optical *and* the magnetic data.

Acknowledgments

The authors thank Dr J P Chaminade and Professor M Pouchard from the Laboratoire de Chimie du Solide du CNRS in Bordeaux for growing the single crystals used in this study and for measurement of the susceptibilities $\chi_\parallel$ and $\chi_\perp$ from 4.2 to 1100 K.

References

[1] Carnall W T, Goodman G L, Rajnak K and Rana R S 1988 A systematic analysis of the spectra of the lanthanides doped into single crystal LaF_3 *Argonne National Laboratory Report*
[2] Caro P, Derouet J, Beaury L, Teste de Sagey G, Chaminade J P, Aride J and Pouchard 1981 *J. Chem. Phys.* **74** 2698
[3] Cheetham A K, Fender B E F, Fuess H and Wright A F 1976 *Acta. Crystallogr.* B **32** 94
[4] Crosswhite H M and Crosswhite H 1984 *J. Opt. Soc. Am.* B **1** 246
[5] Wybourne B G 1965 *Spectroscopic Properties of Rare Earths* (New York: Interscience)
[6] Morrison C A and Leavitt R P 1979 *J. Chem. Phys.* **71** 2366
[7] Duan M and Xu Y 1992 *J. Magn. Magn. Mater.* **115** 1
[8] Porcher P, Svoronos D R, Leskelä M and Hölsä J 1983 *J. Solid State Chem.* **46** 101
[9] Mulay L N 1963 *Magnetic Susceptibility* (New York: Wiley) p 1782
[10] Picard J, Guillot M, Le Gall H, Leycuras C and Feldmann P 1979 *C. R. Acad. Sci.* B **288** 175
[11] Van Vleck J H 1932 *The Theory of Electric and Magnetic Susceptibilities* (Oxford: Oxford University Press)
[12] Beaury L and Caro P 1990 *J. Physique* **51** 471
[13] Baker J M and Rubin R S 1961 *Proc. Phys. Soc.* **78** 1353
[14] Korczak W, Paradowski M L and Misiak L E 1991 *Phys. Status Solidi* b **165** 203

[15] Bauerle D, Borstel G and Sievers A J 1978 *J. Appl. Phys.* 49 676
[16] Bailleul S and Porcher P 1989 *Mol. Phys.* **66** 605
[17] Caro P, Derouet J and Porcher P 1985 *C. R. Acad. Sci.* II **301** 901
[18] Antson O, Beaury L, Derouet J, Hölsä J and Mutka H *Phys. Rev.* to be published